Supporting Information

Facile synthesis of oxygen-deficient nano-TiO_2 coordinated by acetate ligands for enhanced visible-light photocatalytic performance

Shaohua Pang[a,c,†], Yunfei Lu[a,b,†], Lin Cheng[a,b], Juming Liu[a,b,c*], Huiyan Ma[a,b], Jucai Yang[a,c], Qiancheng Zhang[a,b]

[a] Inner Mongolia Key Laboratory of Theoretical and Computational Chemistry Simulation, Inner Mongolia University of Technology, Hohhot 010051, China.

[b] School of Chemical Engineering, Inner Mongolia University of Technology, Hohhot 010051, China.

[c] School of Energy and Power Engineering, Inner Mongolia University of Technology, Hohhot 010051, China.

† These authors contributed equally to this work (co-first authors).

Corresponding author E-mail addresses: liujuming@imut.edu.cn

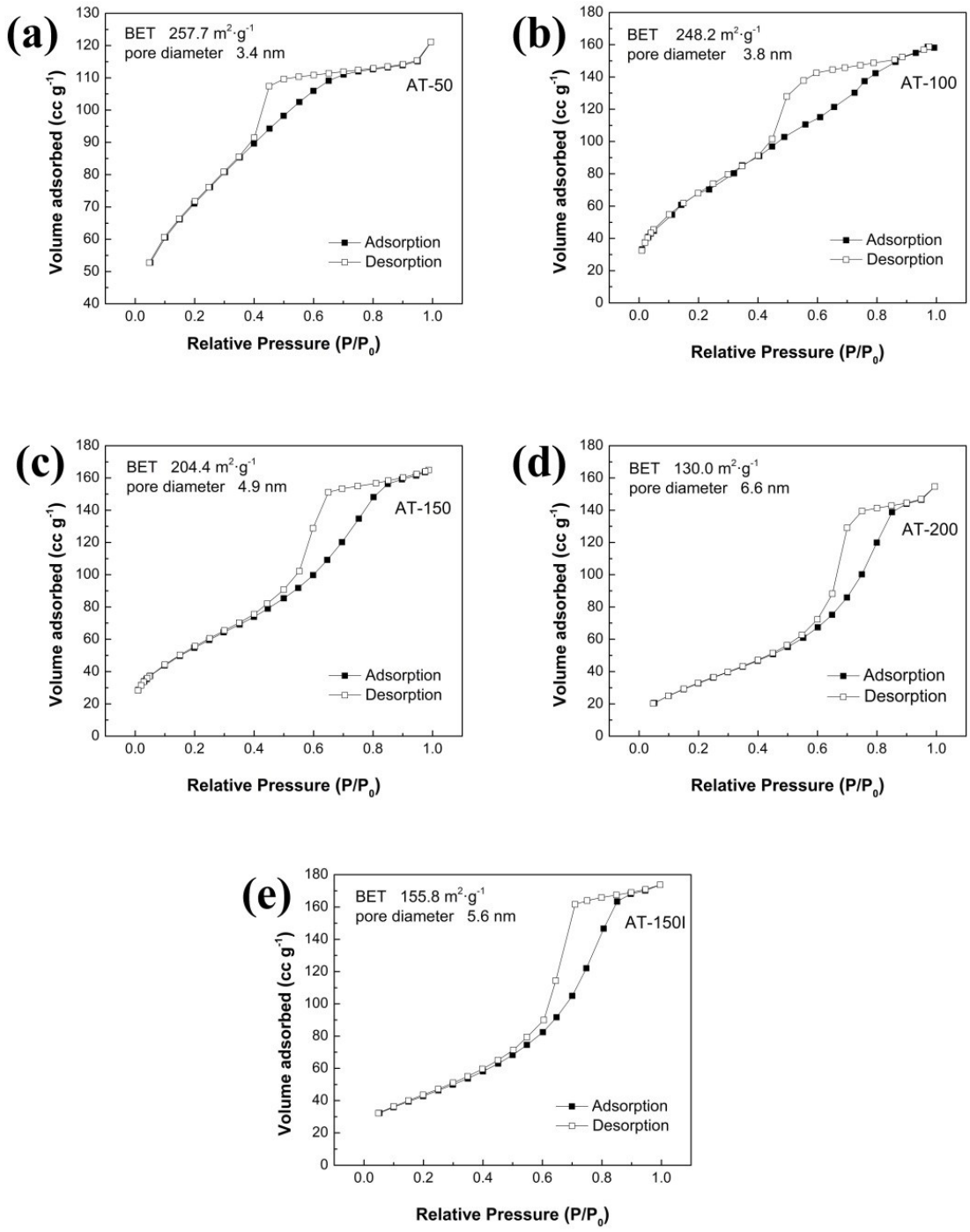

Fig. S1 N_2 adsorption-desorption isotherms, BET surface areas and pore diameters of the as-prepared samples.

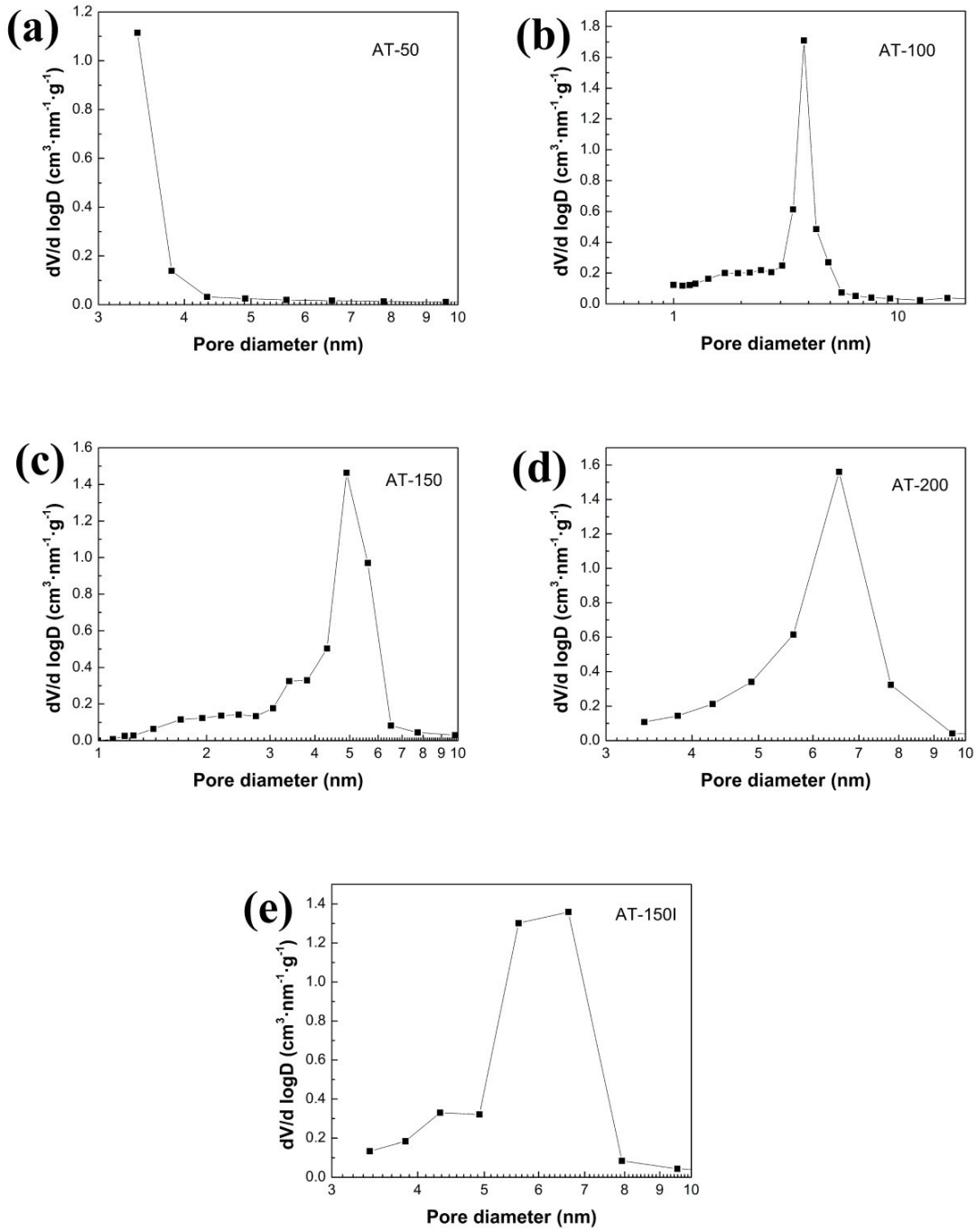

Fig. S2 Pore size distribution of the as-prepared samples.

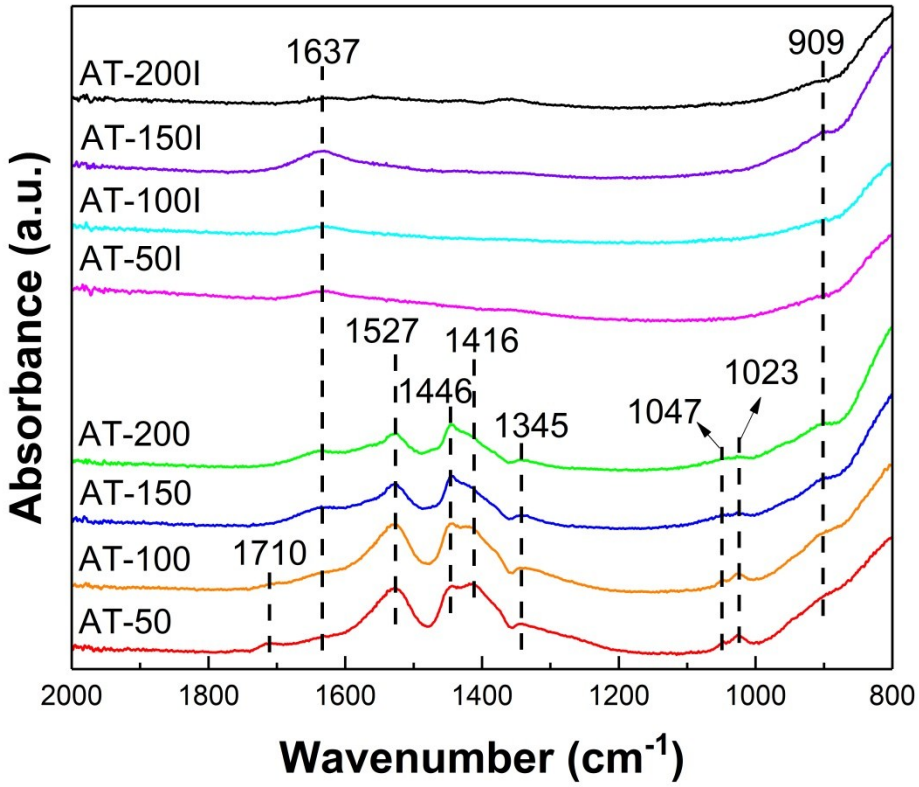

Fig. S3 ATR-FTIR spectra of the as-prepared samples before and after the removal of SALs by the photothermocatalysis method.

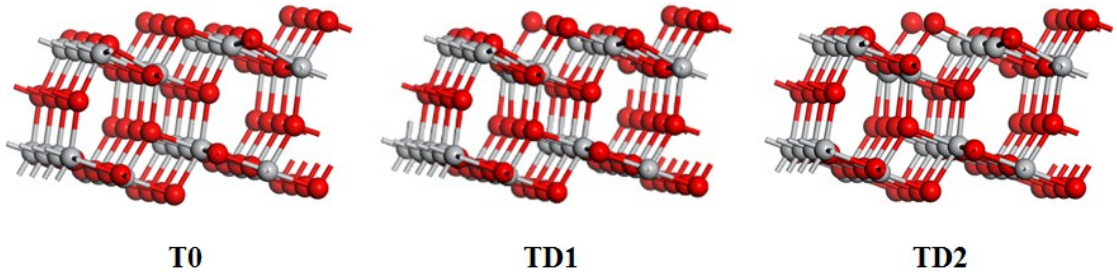

Fig. S4 Three different configurations: pure anatase TiO_2 (101) surface (T0), defective TiO_2 with one oxygen vacancy (TD1) and defective TiO_2 with two oxygen vacancies (TD2). The light gray and red balls represent Ti and O atoms, respectively.

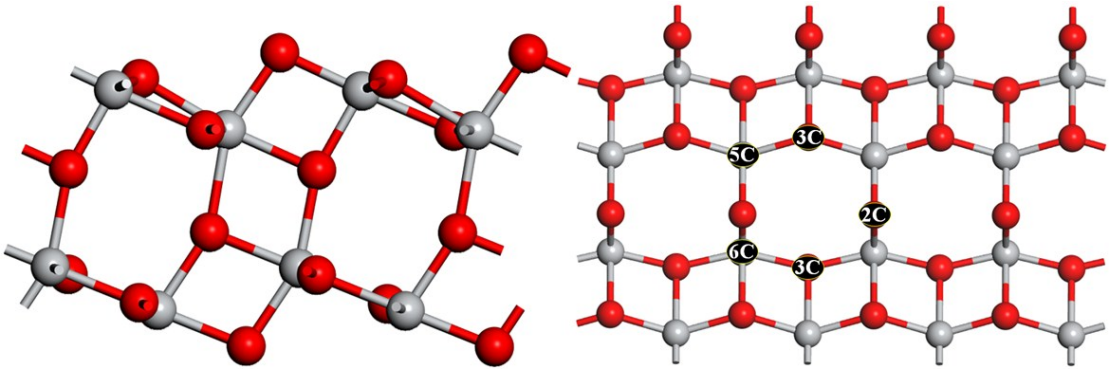

Fig. S5. Side view and top view of pure anatase TiO_2 (101) surface. The light gray and red balls represent Ti and O atoms, respectively.

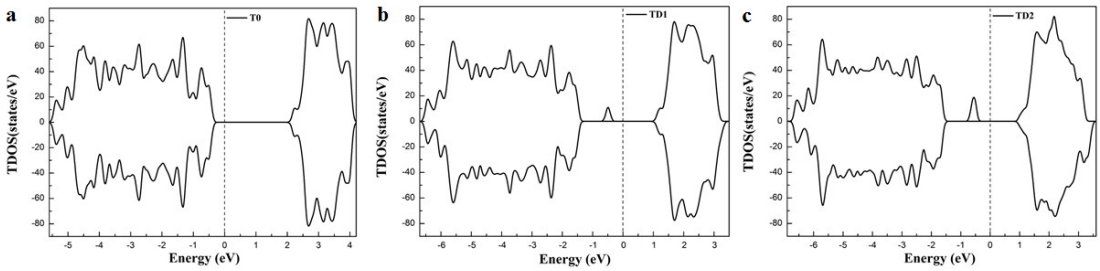

Fig. S6. Total density of states (TDOS) plots of T0, TD1 and TD2. The black dotted line represents the Fermi energy level (E_f).

Table S1. The bandgap (Eg), valance band position (VB), conduction band position (CB) and adsorption energy (ΔE^{ads}) of all configurations.

Configuration	E_g (eV)	VB (eV)	CB (eV)	ΔE^{ads} (eV)
T0	2.37	-0.33	2.04	-
TD1	2.40	-1.41	0.99	-
TD2	2.43	-1.51	0.92	-
ATD1-1	2.19	-1.43	0.76	-6.87
ATD1-2	2.30	-1.54	0.76	-6.12
ATD2-1	2.31	-1.54	0.77	-6.86
ATD2-2	2.24	-1.56	0.68	-

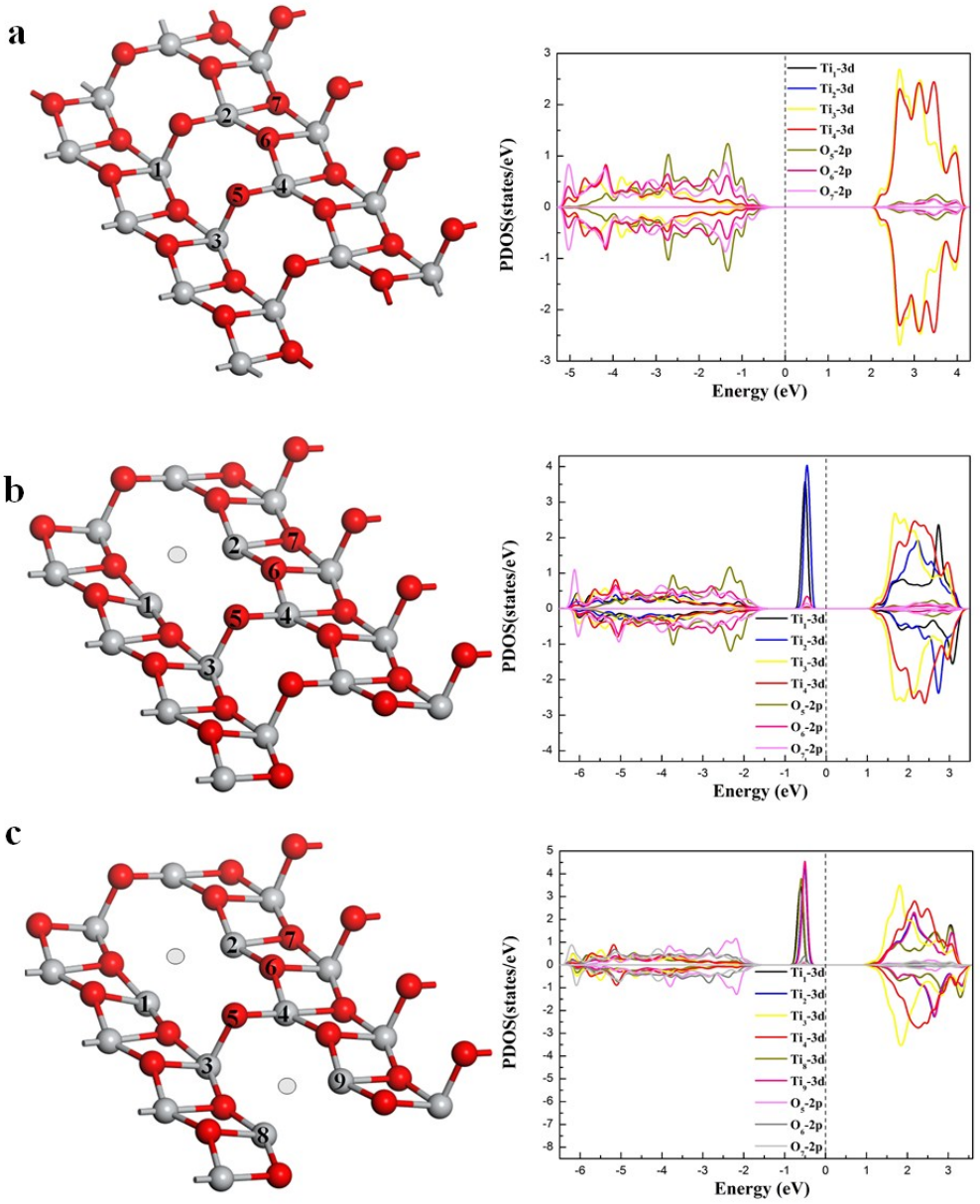

Fig. S7. Partial density of states (PDOS) plots of T0, TD1 and TD2. The black dotted line is the Fermi energy level (E_f). The light gray and red balls represent Ti and O atoms, respectively. The light gray circle represents the oxygen vacancy defect.

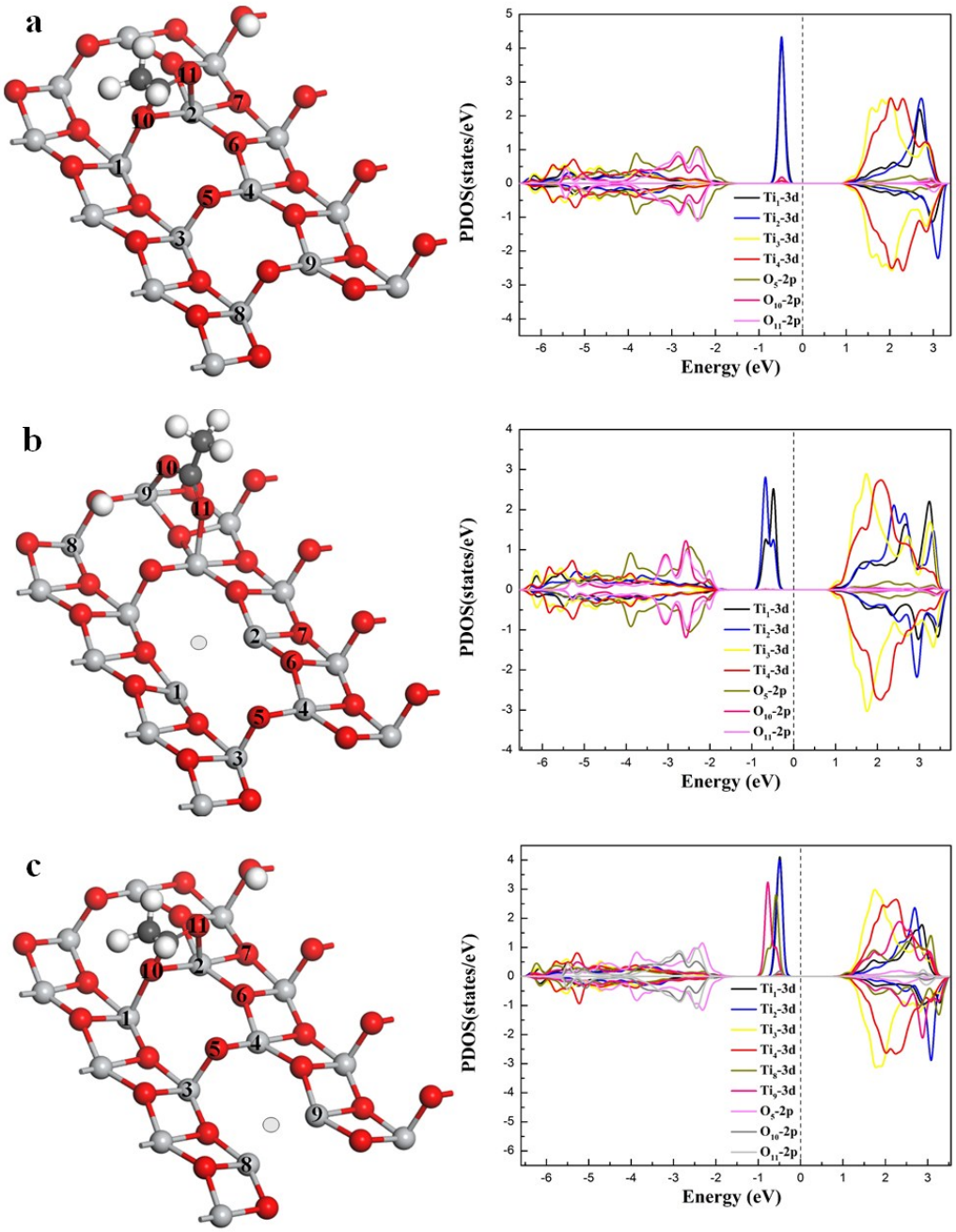

Fig. S8. PDOS plots of ATD1-1, ATD1-2 and ATD2-1. The black dotted line is the Fermi energy level (E_f). The white, dark gray, light gray and red balls represent H, C, Ti and O atoms, respectively. The light gray circle represents the oxygen vacancy defect.

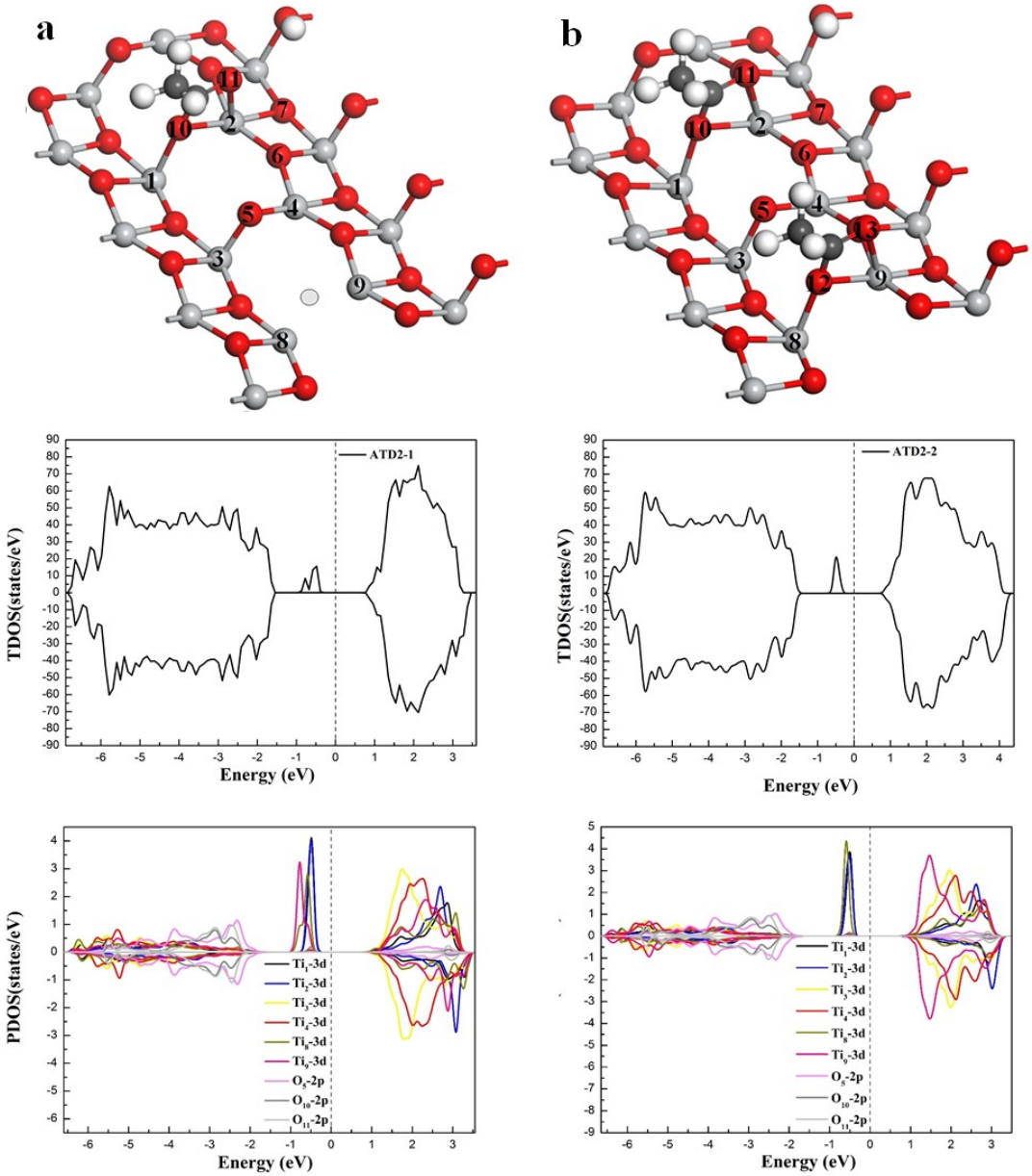

Fig. S9. TDOS and PDOS plots of ATD2-1 and ATD2-2. The black dotted line is the Fermi energy level (E_f). The white, dark gray, light gray and red balls represent H, C, Ti and O atoms, respectively. The light gray circle represents the oxygen vacancy defect.

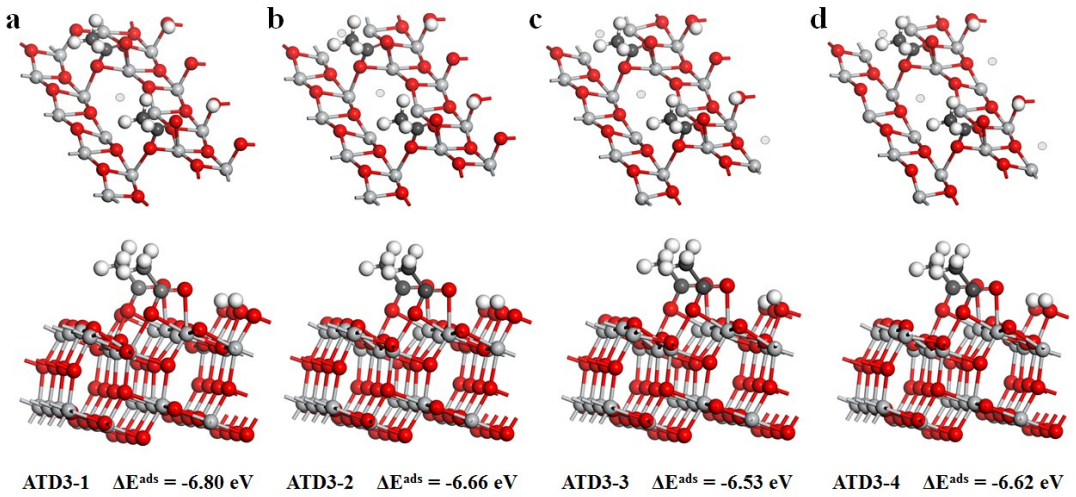

Fig. S10. Some extreme configurations with more acetate ligands and SOVDs: ATD3-1, ATD3-2, ATD3-3 and ATD3-4. The white, dark gray, light gray and red balls represent H, C, Ti and O atoms, respectively. The light gray circle represents the oxygen vacancy defect.

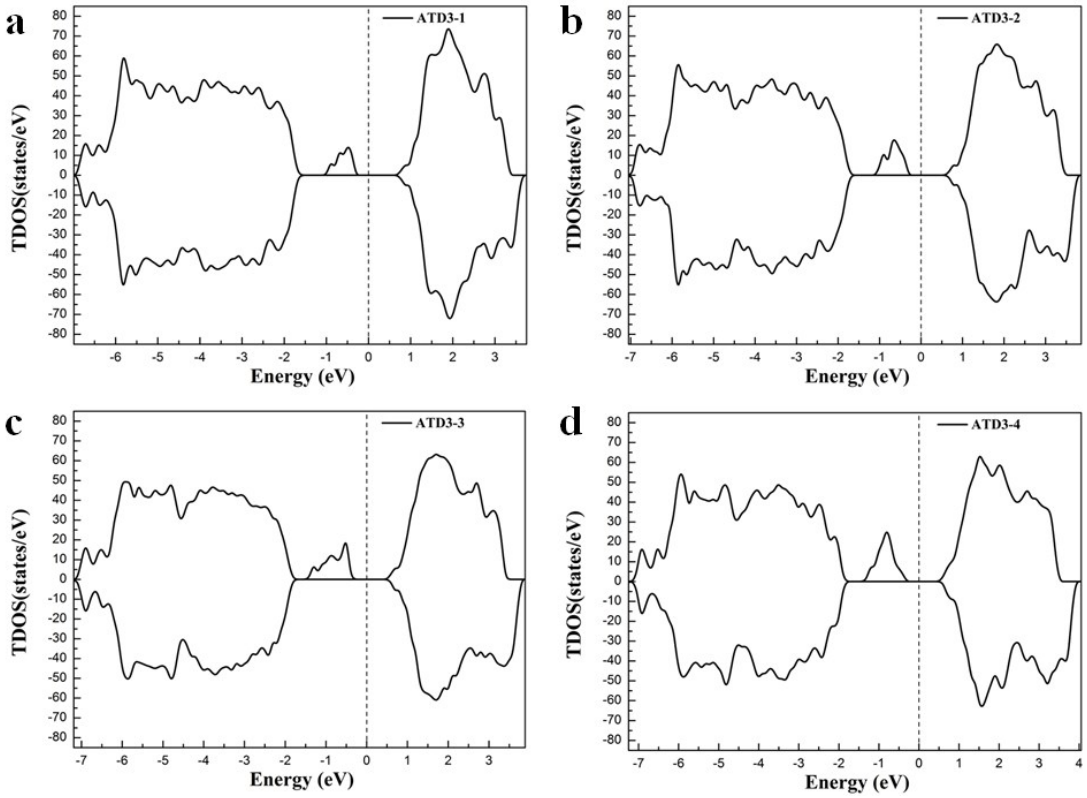

Fig. S11. TDOS plots of ATD3-1, ATD3-2, ATD3-3 and ATD3-4. The black dotted line represents the Fermi energy level (E_f).

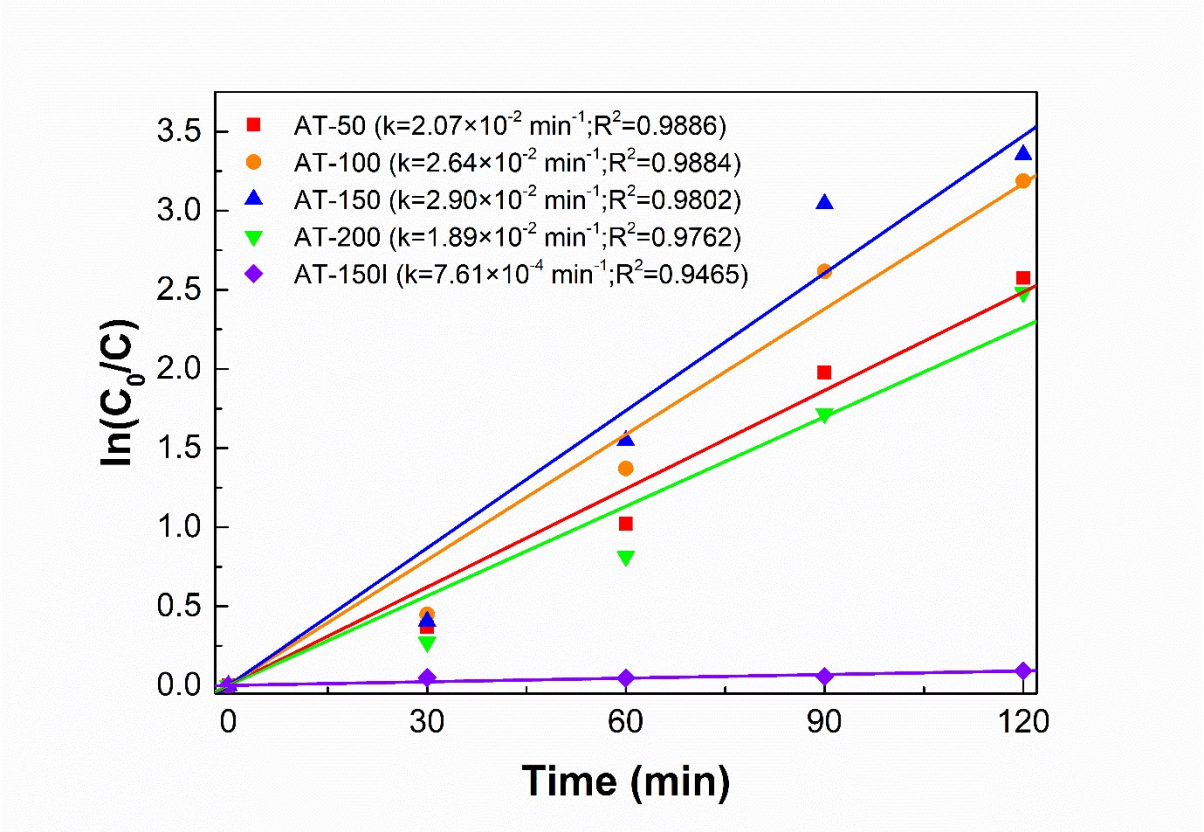

Fig. S12 Plot of ln(C_0/C) versus reaction time for photocatalytic degradation of phenol using the as-prepared samples.

The reaction can be explained by a pseudo-first-order pattern, with the following equation demonstrating the relationship of *C* and *t*:

$$\ln\left(C_0/C\right) = kt$$

where *k* is the apparent reaction rate constant, *t* is the reaction time, C_0 is the initial concentration of phenol in aqueous solution and *C* is the residual concentration of phenol at time *t*. The value of *k* is determined based on the slope obtained by linear fitting the functional relationship between ln(C_0/*C*) and *t*.

Table S2 Comparison of photocatalysts reported in the literature similar to the AT-150 sample for photocatalytic degradation of phenol.

Year of publication	Modification of TiO_2	Mass concentration of photocatalyst (g/L)	Phenol concentration (ppm)	Light source	Light source power (W)	Irradiation time (h)	Degradation activity (%)	Average mass of phenol degraded per gram of photocatalyst per hour (mg / g • h)	References
2020	Doped with carbon	1.0	50	Halogen lamp	250	5	46.6	4.66	1
2018	Doped with nitrogen	0.50	500	F8T5ww lamp	/	7	39.0	55.74	2
2018	phenol-formaldehyde resin-coupled TiO_2	2.0	10	UV lamp (365 nm)	100	2.5	52.0	1.04	3
2018	Modified by carbon dots	1.0	10	Xenon lamp	300	3	nearly 100.0	3.33	4
2017	Hydroxide-TiO_2 Compounds	1.0	10	UV lamp (264 nm)	4	2	12.0	0.60	5
2017	Modified by sulfation, fluorination and platinum	1.0	50	UV lamp (365 nm)	300	2	nearly 100.0	25.00	6
2016	Modified by graphene and heteropoly acid	1.0	50	Tungsten lamp	100	6	85.0	7.08	7
2014	Modified by 7,7,8,8-Tetracyanoquinodimethane (TCNQ)	0.045	20	Xenon lamp (450 nm)	500	8	20.0	11.11	8
2014	Doped with carbon and wrapped by nanographene	1.5	10	Xenon lamp (> 420 nm)	300	3	96.3	2.14	9
2013	Modified by carbon	1.0	1	Low-pressure UV fluorescent tube (254 nm)	8	2.5	100.0	0.40	10
2012	Doped with fluorine	0.50	50	UV lamp (365 nm)	/	1	96.0	96.00	11
2012	Modified by carbon	1.0	20	Xenon lamp (	300	2	60.0	6.00	12

				> 420 nm)					
2007	Modified by poly-(fluorene-co-thiophene) (PFT)	1.0	10	GaI_3 lamp	250	10	75.0	0.75	13
2004	Doped with nitrogen	0.50	20	Xenon lamp (> 400 nm)	1000	2	35.6	7.12	14
/	Co-modified by surface oxygen vacancy defects and surface acetate ligands	3.3	20	Blue LED (450 nm)	20	3	97.2	1.94	This work

1. D. Cherni, S. Ayedi, I. Jaouali, N. Moussa and M. F. Nsib, *Reaction Kinetics, Mechanisms and Catalysis*, 2020, **129**, 1091-1102.
2. T. Boningari, S. N. R. Inturi, M. Suidan and P. G. Smirniotis, *Journal of Materials Science & Technology*, 2018, **34**, 1494-1502.
3. H. Li, J. Ji, C. Cheng and K. Liang, *Journal of Physics and Chemistry of Solids*, 2018, **122**, 25-30.
4. W. Zhang, Y. Zhou, C. Dong, B. Shen, M. Xing and J. Zhang, *Research on Chemical Intermediates*, 2018, **44**, 4797-4807.
5. J. C. Contreras-Ruiz, S. Martínez-Gallegos, E. Ordoñez, J. C. González-Juárez and J. L. García-Rivas, *Journal of Electronic Materials*, 2017, **46**, 1658-1668.
6. J. J. Murcia, M. C. Hidalgo, J. A. Navío, J. Araña and J. M. Doña-Rodríguez, *Applied Catalysis B: Environmental*, 2015, **179**, 305-312.
7. E. Rafiee, E. Noori, A. A. Zinatizadeh and H. Zangeneh, *RSC Adv.*, 2016, **6**, 96554-96562.
8. W. Jiang, M. Zhang, J. Wang, Y. Liu and Y. Zhu, *Applied Catalysis B: Environmental*, 2014, **160-161**, 44-50.
9. S. Yu, H. J. Yun, Y. H. Kim and J. Yi, *Applied Catalysis B: Environmental*, 2014, **144**, 893-899.
10. Y. A. Shaban, *Desalination and Water Treatment*, 2015, **53**, 737-745.
11. C. Yu, Q. Fan, Y. Xie, J. Chen, Q. shu and J. C. Yu, *Journal of Hazardous Materials*, 2012, **237-238**, 38-45.
12. Y. Zhang, P. Zhang, Y. Huo, D. Zhang, G. Li and H. Li, *Applied Catalysis B: Environmental*, 2012, **115-116**, 236-244.
13. L. Song, R. Qiu, Y. Mo, D. Zhang, H. Wei and Y. Xiong, *Catalysis Communications*, 2007, **8**, 429-433.
14. Z. Wang, W. Cai, X. Hong, X. Zhao, F. Xu and C. Cai, *Applied Catalysis B: Environmental*, 2005, **57**, 223-231.

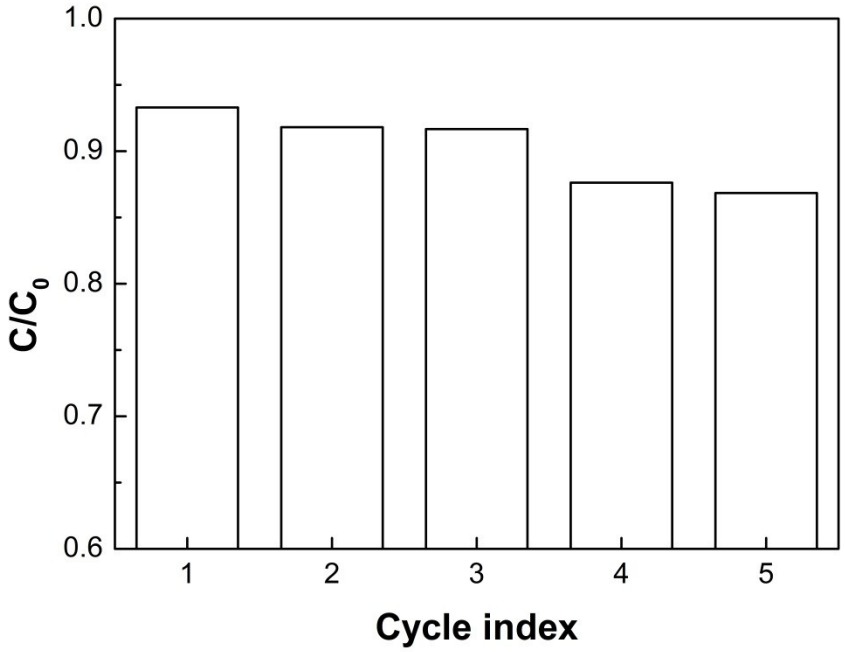

Fig. S13 Recycling properties of AT-150 in the photocatalytic degradation of phenol.

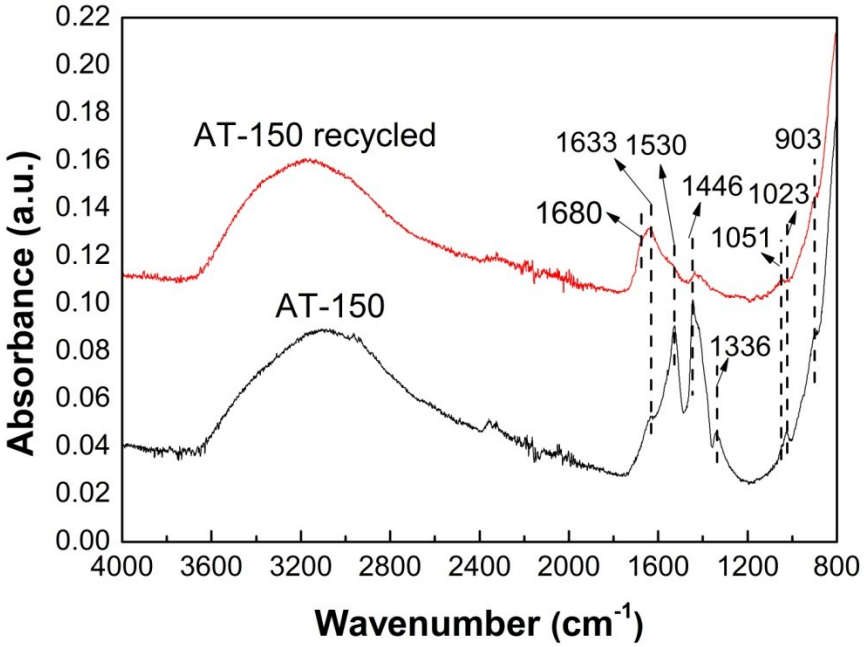

Fig. S14 ATR-FTIR spectra of the AT-150 sample before and after being used.

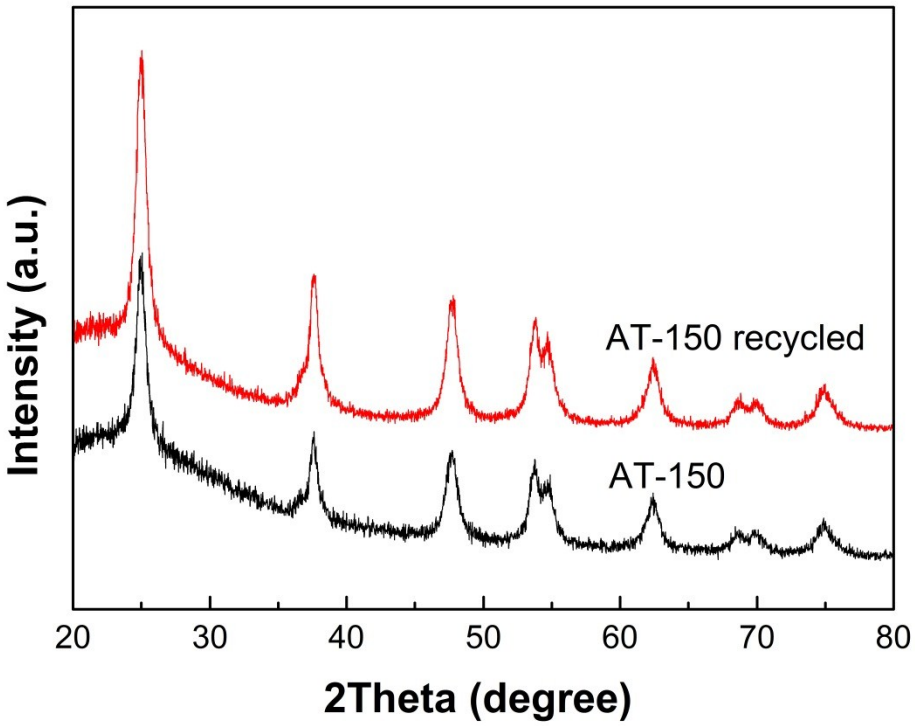

Fig. S15 XRD patterns of the AT-150 sample before and after being used.

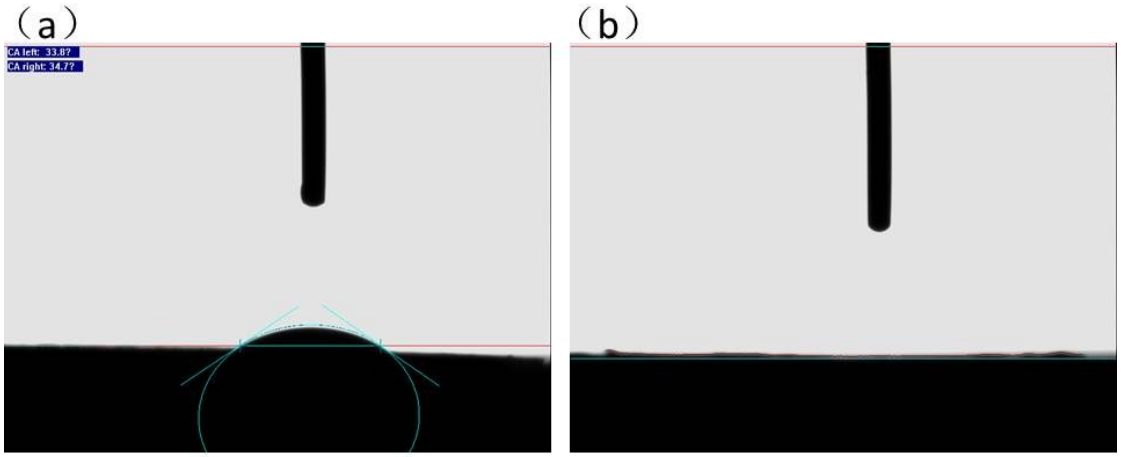

Fig. S16 Contact angle images of (a) AT-150 and (b) AT-150I